




Article

Electronically Tunable Mixed-Mode Universal Filter Employing a Single Active Block and a Minimum Number of Passive Components

Mohammad Faseehuddin ¹, Norbert Herencsar ^{2,*}, Musa Ali Albri ³ and Jahariah Sampe ³

¹ Faculty of Engineering, Symbiosis Institute of Technology (SIT), Symbiosis International University (SIU), Pune, Maharashtra 412115, India; faseehuddin03@gmail.com

² Department of Telecommunications, Brno University of Technology, Technicka 3082/12, 616 00 Brno, Czech Republic

³ Level 4 MINES Lab UKM, Institute of Microengineering and Nanoelectronics (IMEN), University Kebangsaan Malaysia (UKM), Bangi 43600, Selangor, Malaysia; albri@siswa.ukm.edu.my (M.A.A.); jahariah@ukm.edu.my (J.S.)

* Correspondence: herencsn@feec.vutbr.cz; Tel.: +420-541-146-981

Featured Application: Active analog filters are widely used for frequency duplexing in radar and radio communication systems, impedance matching in power amplifiers, anti-aliasing in data converters and in many other areas.

Abstract: A recently developed active building block, namely Voltage Differencing Extra X Current Conveyor (VD-EXCCII), is employed in the design of multi input single output (MISO), electronically tunable mixed-mode universal filter. The filter provides low pass (LP), high pass (HP), band pass (BP), band reject (BR) and all pass (AP) responses in current-mode (CM), voltage-mode (VM), trans-impedance-mode (TIM) and trans-admittance-mode (TAM). The filter employs a single VD-EXCCII, three resistors and two capacitors. Additionally, a CM single input multi output (SIMO) filter can be derived from the same circuit topology by only adding current output terminals. The attractive features of the filter include: (i) the ability to operate in all four modes, (ii) the tunability of the Q factor independent of pole frequency, (iii) the low output impedance for the VM filter, (iv) the high output impedance current output for CM and TAM filters and (v) no requirement for double/negative input signals (voltage/current) for response realization. The VD-EXCCII and its layout is designed and validated in Cadence Virtuoso using 0.18 μm pdk from Silterra Malaysia with a supply voltage of ± 1.25 V. The operation of the filter is examined at the 8.0844 MHz characteristic frequency. A non-ideal parasitic and sensitivity analysis is also carried out to study the effect of process and components spread on the filter performance.

Keywords: communication; current conveyor; current-mode; mixed-mode; voltage-mode; universal filter; signal processing; VD-EXCCII



Citation: Faseehuddin, M.; Herencsar, N.; Albri, M.A.; Sampe, J. Electronically Tunable Mixed-Mode Universal Filter Employing a Single Active Block and a Minimum Number of Passive Components. *Appl. Sci.* **2021**, *11*, 55. <https://dx.doi.org/10.3390/app11010055>

Received: 7 October 2020

Accepted: 2 December 2020

Published: 23 December 2020

Publisher's Note: MDPI stays neutral with regard to jurisdictional claims in published maps and institutional affiliations.



Copyright: © 2020 by the authors. Licensee MDPI, Basel, Switzerland. This article is an open access article distributed under the terms and conditions of the Creative Commons Attribution (CC BY) license (<https://creativecommons.org/licenses/by/4.0/>).

1. Introduction

The current-mode (CM) active building blocks (ABBs) are widely employed in designing universal frequency filters. The CM ABBs exhibits greater linearity, wide bandwidth, simple structure, low power consumption and enhanced dynamic range [1–5]. Extensive number of filter topologies using CM ABBs can be found in the literature. However, the majority of the previously proposed filters can work only in single mode of operation i.e., CM, voltage-mode (VM), trans-impedance-mode (TIM) or trans-admittance-mode (TAM) [1–3,5]. In present-day intricate signal processing systems, the interaction between CM and VM circuits is required. This task can be accomplished by TAM and TIM filters that not only perform signal processing, but also provide interfacing between VM and CM systems [6–10]. The development of mixed-mode universal filters that can provide low

pass (LP), high pass (HP), band pass (BP), band reject (BR) and all pass (AP) filter responses in CM, VM, TAM and TIM modes of operation are best suited for the task.

Numerous exemplary mixed-mode filter structures have been developed that employ different variants of the CM ABBs [8–12]. The filters can be segregated in two broad categories single input multi output (SIMO) and multi input single output (MISO) type. The MISO filter configuration is one of the most sought after. The filters can be compared on many criteria, some important measures of comparison are: (i) number of ABBs employed, (ii) number of passive components needed, (iii) employment of all grounded passive components, (iv) no requirement for resistive matching except for AP response, (v) provision to control quality factor (Q) independent of the center frequency, (vi) ability to provide all five filter responses in all four modes of operation, (vii) low output impedance for VM mode, (viii) availability of explicit current output in CM and TAM modes, (ix) no requirement for double/negative input signals (voltage/current), (x) inbuilt tunability and (xi) test frequency. A detailed comparison of the state-of-the-art MISO filters with the proposed design is presented in Table 1 [6–39] and Table 2 [7,9,12,13,19,20,24–27,29,37–41]. It can be inferred from the tables that the filter structures in [6–13,15–24,26,28–39] employ more than one ABB. The designs in [6,7,10,12,22,28–30,36,37,39,41] use more than five passive components. The filter structures proposed by [6,7,9–13,18,19,21,24,25,27,30,32,33,36,39] do not provide frequency control independent of quality factor. The filter structures [6,8,9,11,13–16,18,21,23,25–28,32,34,35,41] do not provide all five filter responses in VM, CM, TAM and TIM operation. The filter structures [6,7,10–12,14,16,22,25,27–30,34,36,37,39,41] lack inbuilt tunability property. In addition, only four mixed mode filter structures [14,25,27,40] employing a single ABB can be currently found in the literature. Moreover, among single ABBs based mixed mode filters only [40] provides all five filter responses in all four modes of operation. Furthermore, the design in [40] does not provide VM response at low impedance node. It can be deduced from the literature survey that a limited number of mixed-mode filters are available, and to fill this technological void, additional novel mixed-mode filter structures are needed.

In the literature, numerous CM ABBs can be found, each having its own merits. In this research, the Voltage Differencing Extra X Current Conveyor (VD-EXCCII) is introduced and utilized in the design of mixed-mode filter. The proposed VD-EXCCII can be considered a universal ABB, as it can realize many popular and widely employed CM ABBs as special case. The proposed VD-EXCCII can realize second generation current conveyor (CCII), voltage differencing current conveyor (VDCC), differential difference current conveyor (DDCC), voltage differencing transconductance amplifier (VDTA), voltage differencing buffered amplifier (VDBA), current backward transconductance amplifier (CBTA) and operational transconductance amplifier (OTA) by proper interconnection of its input and output terminals, thereby making it an inherently universal ABB. This will allow designers to employ VD-EXCCII instead of using each separate ABBs to test their designs, thus reducing the cost and time to market. The filter design requires a single VD-EXCCII, two capacitors and three resistors. The striking features of the proposed filters are: (i) employment of single active block (VD-EXCCII), (ii) ability to work in all four modes of operation, (iii) provision for inbuilt tunability, (iv) the filter enjoy low active and passive sensitivities. Moreover, the filter enjoy all (iv–x) properties mentioned in Table 2. The design simulation of the VD-EXCCII is done in Cadence Virtuoso using Silterra Malaysia 0.18 μm PDK. The post-layout simulation results are in good agreement with the theoretical predictions.

Table 1. Comparative study of the state-of-the-art mixed-mode designs.

References	Number of ABBs	Filter Responses Realized				Passive Components		Inbuilt Tunability	Control of Q Independent of Frequency	Grounded Passive Components
		VM	CM	TAM	TIM	R	C			
[6]/2004	5-CCII	All Five	All Five	-	-	7	2	No	No	No
[7]/2004	7-CCII	All Five	All Five	All Five	All Five	8	2	No	No	No
[8]/2003	4-CCCII	HP, BP, LP, BR	HP, BP, LP, BR	HP, BP, LP, BR	HP, BP, LP, BR	0	2	Yes	Yes	Yes
[9]/2003	6-OTA	All Five	All Five	-	-	0	2	Yes	No	Yes
[10]/2005	4-CFOA	All Five	All Five	All Five	All Five	9	2	No	No	No
[11]/2006	2-FTFN	HP, BP, LP	HP, BP, LP	HP, BP	BP, LP	3	2	No	No	No
[12]/2006	3-CCII	All Five	All Five	All Five	All Five	4	3	No	No	No
[13]/2008	4-OTA	HP, BP, LP	All Five	All Five	HP, BP, LP	0	2	Yes	No	Yes
[14]/2009	1-FDCCII	All Five	All Five	BP, HP	All Five	3	2	No	Yes	No
[15]/2009	5-MOCCII	HP, BP, LP	HP, BP, LP	HP, BP, LP	HP, BP, LP	0	2	Yes	Yes	Yes
[16]/2009	3-DVCC	LP, BP, BR	All Five	All Five	BP, LP	3	2	No	Yes	Yes
[17]/2009	5-OTA	All Five	All Five	All Five	All Five	0	2	Yes	Yes	Yes
[18]/2011	3-CCCCTA	HP, LP, BP	All Five	All Five	HP, LP, BP	0	2	Yes	No	Yes
[19]/2010	5-OTA	All Five	All Five	All Five	All Five	0	2	Yes	No	Yes
[20]/2010	2-MOCCII	All Five	All Five	All Five	All Five	2	2	Yes	Yes	No
[21]/2010	2-CCCCTA	LP, BP	All Five	All Five	LP, BP	0	2	Yes	No	No
[22]/2011	3-DDCC	All Five	All Five	All Five	All Five	4	2	No	Yes	No
[23]/2012	6-OTA	All Five	All Five	HP, BP	All Five	0	2	Yes	Yes	Yes
[24]/2013	4-MOCCII	All Five	All Five	All Five	All Five	0	2	Yes	No	Yes
[25]/2013	1-FDCCII	All Five	HP, BP, LP	HP, BP	LP, BP	2	2	No	No	No
[26]/2013	2-VDTA	All Five	-	All Five	-	0	2	Yes	Yes	Yes
[27]/2010	1-CFOA	All Five	BR, BP, LP	-	-	3	2	No	No	No
[28]/2015	3-DDCC	HP, BP, LP	HP, BP, LP	-	-	5	3	No	Yes	No
[29]/2016	1-FDCCII+, 1-DDCC	All Five	All Five	All Five	All Five	6	2	No	Yes	No
[30]/2016	2-FDCCII	All Five	All Five	All Five	All Five	5	2	No	No	No
[31]/2017	3-CCCCTA	All Five	All Five	All Five	All Five	0	2	Yes	Yes	Yes
[32]/2017	3-VDTA	HP, LP, BP	-	All Five	-	0	2	Yes	No	Yes
[33]/2017	6-OTA	All Five	All Five	All Five	All Five	0	2	Yes	No	Yes
[34]/2017	1-DVCC+, 1MOCCII	-	All Five	-	All Five	3	2	No	Yes	No
[35]/2017	4-OTA	-	All Five	All Five	-	0	2	Yes	Yes	Yes
[36]/2018	2-FDCCII	All Five	All Five	All Five	All Five	4	2	No	No	No
[37]/2018	5-DVCCII	All Five	All Five	All Five	All Five	5	2	No	Yes	Yes
[38]/2019	5-OTA	All Five	All Five	All Five	All Five	0	2	Yes	Yes	Yes
[39]/2020	3-DDCC	All Five	All Five	All Five	All Five	4	2	No	No	No
This work	1-VD-EXCCII	All Five	All Five	All Five	All Five	3	2	Yes	Yes	No

Note: ‘-’ Cannot function in the given mode of operation.

2. Voltage Differencing Extra X Current Conveyor (VD-EXCCII)

The proposed Voltage Differencing Extra X current conveyor (VD-EXCCII) is derived by connecting extra X second generation current conveyor (EXCCII) [42] and operational transconductance amplifier (OTA). The first stage comprises of OTA followed by the CCII with two current input terminals. The developed active element has characteristics of CCII and tunable OTA in one structure. The voltage-current (V-I) characteristics of the developed VD-EXCCII are presented in Equations (1)–(4) and the block diagram is presented in Figure 1.

$$I_W = I_{WC+} = -I_{WC-} = g_{m1}(V_P - V_N) \tag{1}$$

$$V_{XP} = V_{XN} = V_W \tag{2}$$

$$I_{XP} = I_{ZP+} = -I_{ZP-} \tag{3}$$

$$I_{XN} = I_{ZN+} = -I_{ZN-} \tag{4}$$

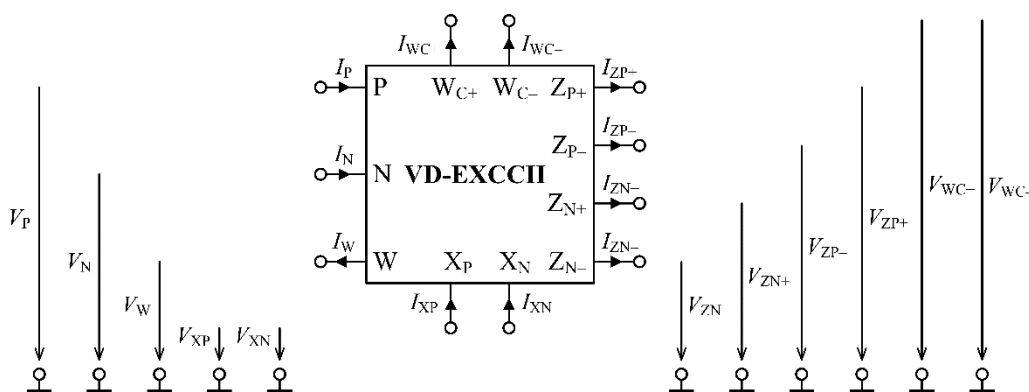


Figure 1. Block diagram of VD-EXCCII.

The CMOS implementation of VD-EXCCII is given in Figure 2. The first stage consists of OTA MOS transistors (M1–M14). The output current of the transconductor depends on the voltage difference ($V_P - V_N$). Assuming that all transistors are operating in saturation region and the transistors (M1–M2) have equal width to length ratio, the output current is given by:

$$I_W = I_{WC+} = -I_{WC-} = g_{m1}(V_P - V_N) = \left(\sqrt{2I_{Bias}K_i}\right)(V_P - V_N) \tag{5}$$

where the transconductance parameter $K_i = \mu C_{ox} \frac{W}{2L}$, ($i = 1, 2$), W is the effective channel width, L is the effective length of the channel, C_{ox} is the gate oxide capacitance per unit area and μ is the carrier mobility.

The second stage is made up of hybrid voltage and current followers (M15–M44). The voltage developed at node W is transferred to nodes X_P and X_N . In the same way the input current from X_P node is transferred to Z_{P+} and Z_{P-} . Furthermore, the input current from X_N node is transferred to Z_{N+} and Z_{N-} . The current flowing in the Z_N and Z_P terminals are independent of each other. The class AB output stage is utilized in the output stage, as it is suitable for low voltage operation and better dynamic range [2]. The current and voltage reference circuits available in the literature [43] can be employed to generate the I_{Bias} and V_{Bias} for the circuit.

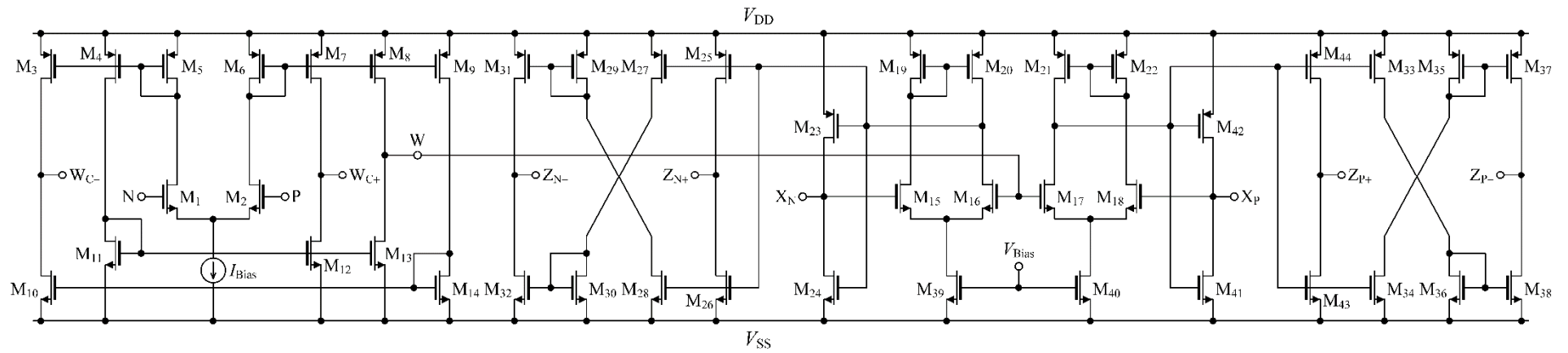


Figure 2. CMOS implementation of VD-EXCCII.

The small signal analysis yields the expression relating V_W , V_{XP} and V_{XN} . The analysis is carried out for the differential stage formed by transistors (M_{15} – M_{24} , M_{39} – M_{42}). The voltage transfer ratio between the W and X_P node can be derived as given in Equation (6).

$$\alpha_P = \frac{V_{XP}}{V_W} = \frac{\frac{r_{039}r_{040}}{r_{039} + r_{040}}(g_{m39} + g_{m40})\frac{r_{0p}}{2}g_{m18}}{\frac{r_{039}r_{040}}{r_{039} + r_{040}}(g_{m39} + g_{m40})\frac{r_{0p}}{2}g_{m17} + 1} \cong \frac{g_{m18}}{g_{m17}} \tag{6}$$

where $r_{0p} = r_{017} // r_{021}$, r_0 is the output resistance of the MOS transistor and g_{mi} is the transconductance of the MOS transistor M_i . Similarly, the voltage transfer gain α_N is computed as:

$$\alpha_N = \frac{V_{XN}}{V_W} \cong \frac{g_{m15}}{g_{m16}} \tag{7}$$

The current transfer ratios are derived as given in Equations (8) and (9):

$$\beta_P = \frac{I_{ZP}}{I_{XP}} = \frac{\frac{\frac{r_{041}r_{042}}{r_{041} + r_{042}}(g_{m41} + g_{m42}) + R_{ZLOAD}}{\frac{r_{039}r_{040}}{r_{039} + r_{040}}(g_{m39} + g_{m40})}}{\frac{\frac{r_{041}r_{042}}{r_{041} + r_{042}}(g_{m41} + g_{m42}) + R_{ZLOAD}}{\frac{r_{039}r_{040}}{r_{039} + r_{040}}(g_{m39} + g_{m40}) + R_{XLOAD}}} \cong \frac{(g_{m41} + g_{m42})}{(g_{m39} + g_{m40})} \tag{8}$$

$$\beta_N = \frac{I_{ZN}}{I_{XN}} \cong \frac{(g_{m25} + g_{m26})}{(g_{m23} + g_{m24})} \tag{9}$$

The terminal resistance of X_N and X_P terminals is calculated as given in Equations (10) and (11). The Z_{P+} , Z_{N+} and W_{C+} resistance are presented in Equations (12)–(14).

$$R_{XP} = \frac{1}{\frac{r_{039}r_{040}}{r_{039} + r_{040}}(g_{m39} + g_{m40})\frac{r_{0p}}{2}g_{m18}} \cong \frac{2}{r_{0p}g_{m18}(g_{m39} + g_{m40})} \tag{10}$$

$$R_{XN} \cong \frac{2}{r_{0n}g_{m15}(g_{m23} + g_{m24})} \tag{11}$$

where $r_{0p} = r_{017} // r_{021}$ and $r_{0n} = r_{016} // r_{020}$.

$$R_{ZP+} = \frac{r_{039}r_{040}}{r_{039} + r_{040}} \tag{12}$$

$$R_{ZN+} = \frac{r_{025}r_{026}}{r_{025} + r_{026}} \tag{13}$$

$$R_{WC+} = \frac{r_{08}r_{013}}{r_{08} + r_{013}} \tag{14}$$

The Z_{P+} , Z_{N+} and W_{C+} node impedances are found to be high given by the parallel output resistance of the MOS transistors.

3. Proposed Electronically Tunable Mixed-Mode Universal Filter

The proposed MISO mixed mode filter is presented in Figure 3. It provides all five filter responses in VM, TAM, TIM and CM modes of operation. The minimum component filter employs a single VD-EXCCII, three resistors and two capacitors. The main attributes of the filter are: (i) use of a single active element, (ii) employment of only five passive components, (iii) no need for capacitive matching condition, (iv) availability of VM output from low impedance terminal, (v) availability of TAM and CM output from high impedance terminals, (vi) no requirement for negative/double input signals for response realization,

(vii) inbuilt tunability of Q independent of frequency and (viii) in TIM mode, the filter gain can be adjusted without affecting ω_0 and Q .

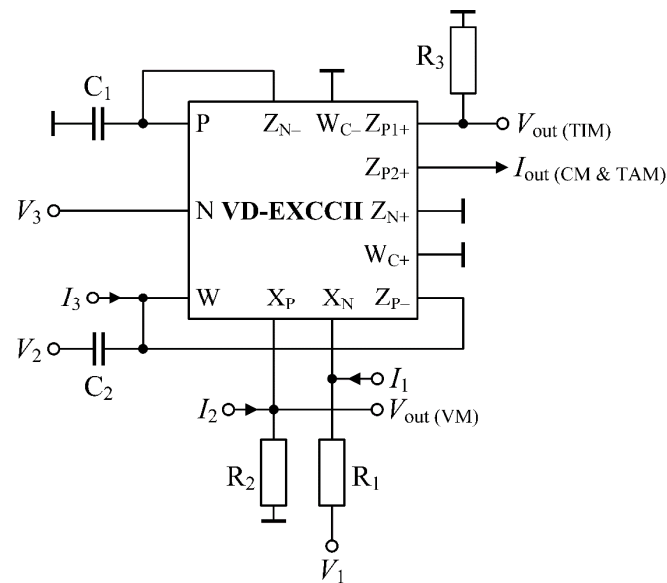


Figure 3. Proposed mixed mode universal filter employing VD-EXCCII.

3.1. Operation in VM and TAM

In this mode of operation, all input currents (I_1 – I_3) are set to zero. The input voltages (V_1 – V_3) are applied as per the sequence given in Table 3. The filter transfer functions and expression for pole frequency and quality factor are given in Equations (15)–(18):

$$V_{out} = \frac{V_1 g_{m1} R_2 - g_{m1} R_2 R_1 s C_1 V_3 + s^2 C_1 C_2 R_1 R_2 V_2}{s^2 C_1 C_2 R_1 R_2 + s C_1 R_1 + g_{m1} R_2} \tag{15}$$

$$I_{out(TAM)} = \frac{1}{R_2} \frac{V_1 g_{m1} R_2 - g_{m1} R_2 R_1 s C_1 V_3 + s^2 C_1 C_2 R_1 R_2 V_2}{s^2 C_1 C_2 R_1 R_2 + s C_1 R_1 + g_{m1} R_2} \tag{16}$$

$$\omega_0 = \sqrt{\frac{g_{m1}}{C_1 C_2 R_1}} \tag{17}$$

$$Q = R_2 \sqrt{\frac{C_2 g_{m1}}{C_1 R_1}} \tag{18}$$

Table 3. Input excitation sequence of operation in VM and TAM.

Response	Inputs			Passive Matching Condition
	V_1	V_2	V_3	
LP	1	0	0	No
HP	0	1	0	No
BP	0	0	1	No
BR	1	1	0	No
AP	1	1	1	$1 = g_{m1} R_2$

The Equations (17) and (18) imply that when the frequency is varied, the quality factor of the filter will be slightly affected. The frequency can be tuned without affecting the quality factor if g_{m1} and R_1 are varied simultaneously such that the product ($R_1 \cdot g_{m1}$) remains constant. The resistor can be realized using a MOS [44] transistor, making it easily tunable.

3.2. Operation in CM and TIM

In CM mode, the input voltages are set to zero. The input currents (I_1 – I_3) are applied according to Table 4 to obtain CM and TIM responses.

Table 4. Input excitation sequence of operation in CM and TIM.

Response	Inputs			Passive Matching Condition
	I_1	I_2	I_3	
LP	1	0	0	No
HP	1	1	0	$R_1 = R_2$
BP	0	0	1	No
BR	0	1	0	No
AP	0	1	1	No

The filter transfer functions are given in Equations (19) and (20):

$$I_{out} = \frac{-(s^2C_1C_2R_1R_2 + g_{m1}R_2)I_2 + sC_1R_1I_3 + g_{m1}R_1I_1}{s^2C_1C_2R_1R_2 + sC_1R_1 + g_{m1}R_2} \tag{19}$$

In TIM mode, the gain of the filter can be varied without disturbing the Q and ω_0 of the filter by varying the value of R_3 , as in the transfer function, R_3 is common to all the responses:

$$V_{out(TIM)} = R_3 \left[\frac{-(s^2C_1C_2R_1R_2 + g_{m1}R_2)I_2 + sC_1R_1I_3 + g_{m1}R_1I_1}{s^2C_1C_2R_1R_2 + sC_1R_1 + g_{m1}R_2} \right] \tag{20}$$

Additionally, the CM SIMO filter shown in Figure 4 is derived from the proposed mixed mode filter by adding additional current output terminals without changing the core topology. All passive components are grounded in CM SIMO configuration. The filter requires a single VD-EXCCII, two resistors and two capacitors, all grounded. The resistor R_3 is not required. since it is needed only to obtain the TIM response. The attractive features of the derived SIMO CM filter include (i) use of single active element, (ii) employment of only three grounded passive components, (iii) no need for passive components matching condition, (iv) low input impedance, (v) high output impedance and (vi) inbuilt tunability.

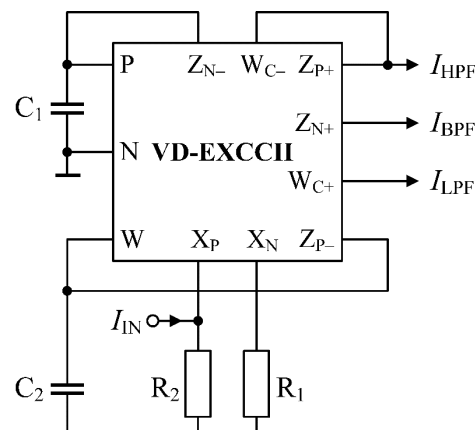


Figure 4. Proposed CM SIMO filter.

The filter transfer functions are given in Equations (21)–(25). Expression for pole frequency and quality factor will be same as that of mixed mode MISO filter given by Equations (17) and (18).

$$\frac{I_{LP}}{I_{IN}} = \frac{-g_{m1}R_2}{s^2C_1C_2R_1R_2 + sC_1R_1 + g_{m1}R_2} \tag{21}$$

$$\frac{I_{HP}}{I_{IN}} = \frac{-s^2C_1C_2R_1R_2}{s^2C_1C_2R_1R_2 + sC_1R_1 + g_{m1}R_2} \tag{22}$$

$$\frac{I_{BP}}{I_{IN}} = \frac{sC_1R_2}{s^2C_1C_2R_1R_2 + sC_1R_1 + g_{m1}R_2} \tag{23}$$

The BR and AP response can be obtained by simply summing the LP, HP and BP currents: $I_{BR} = I_{HP} + I_{LP}$ and $I_{AP} = I_{HP} + I_{LP} + I_{BP}$.

$$\frac{I_{NP}}{I_{IN}} = \frac{-g_{m1}R_2 - s^2C_1C_2R_1R_2}{s^2C_1C_2R_1R_2 + sC_1R_1 + g_{m1}R_2} \tag{24}$$

$$\frac{I_{AP}}{I_{IN}} = \frac{-g_{m1}R_2 - s^2C_1C_2R_1R_2 + sC_1R_2}{s^2C_1C_2R_1R_2 + sC_1R_1 + g_{m1}R_2} \tag{25}$$

4. Non-Ideality and Sensitivity Analysis

4.1. Non-Ideal Gain and Sensitivity Analysis

The non-ideal effects that influences the response of the VD-EXCCII are the frequency-dependent non-ideal current ($\alpha_{P/N}$, $\alpha'_{P/N}$), voltage ($\beta_{P/N}$) and transconductance transfer (γ , γ') gains. These non-ideal gains result in a change in the current and voltage signals during transfer leading to undesired response. Taking into account the non-ideal gains, the V–I characteristics of the VD-EXCCII in (1–4) will be modified as follows: $I_W = 0$, $V_{XP} = \beta_P V_W$, $V_{XN} = \beta_N V_W$, $I_{ZP+} = \alpha_P I_{XP}$, $I_{ZP-} = \alpha'_P I_{XP}$, $I_{ZN+} = \alpha_N I_{XN}$, $I_{ZN-} = \alpha'_N I_{XN}$, $I_W = I_{WC+} = \gamma g_{m1}(V_P - V_N)$, $I_{WC-} = -\gamma' g_{m1}(V_P - V_N)$, where $\beta_{(P,N)} = 1 - \varepsilon_{v(P,N)}$, $\alpha_P = 1 - \varepsilon_{iP}$, $\alpha_N = 1 - \varepsilon_{iN}$, $\gamma = 1 - \varepsilon_{g_{m1}}$ and $\gamma' = 1 - \varepsilon'_{g_{m1}}$. Here, $\varepsilon_{v(P,N)} \left(\left| \varepsilon_{v(P,N)} \right| \ll 1 \right)$ denote voltage tracking errors, ε_{iP} , ε_{iN} ($|\varepsilon_{iP}|$, $|\varepsilon_{iN}| \ll 1$) denote current tracking errors and $\varepsilon_{g_{m1}}$, $\varepsilon'_{g_{m1}}$ ($|\varepsilon_{g_{m1}}|$, $|\varepsilon'_{g_{m1}}| \ll 1$) denote transconductance errors of the VD-EXCCII.

The non-ideal analysis considering the effect of non-ideal current, voltage and transconductance transfer gains is carried out for VM, CM, TAM and TIM configurations to see its effect on the transfer function, f_0 and Q of the proposed filters. The modified expressions of the filter transfer functions, f'_0 and Q' for the MISO/ SIMO configurations are presented in Equations (26)–(31):

$$V'_{out(VM-Mode)} = \left[\frac{s^2C_1C_2R_1R_2V_2 - Yg_{m1}sC_1R_1R_2V_3 + \alpha'_N Yg_{m1}R_1R_2V_1}{s^2C_1C_2R_1R_2 + \alpha'_P \beta_P sC_1R_1 + \beta_N \alpha'_N Yg_{m1}R_2} \right] \tag{26}$$

$$I'_{out(TAM-Mode)} = \frac{\alpha_P \beta_P}{R_2} \left[\frac{s^2C_1C_2R_1R_2V_2 - Yg_{m1}sC_1R_1R_2V_3 + \alpha'_N Yg_{m1}R_1R_2V_1}{s^2C_1C_2R_1R_2 + \alpha'_P \beta_P sC_1R_1 + \beta_N \alpha'_N Yg_{m1}R_2} \right] \tag{27}$$

$$I'_{out(CM-Mode)} = \left[\frac{-\alpha_P [s^2C_1C_2R_1R_2 + \beta_P \alpha'_P sC_1R_1 + \beta_N \alpha'_N Yg_{m1}R_2] I_2 + \alpha_P \beta_P \alpha'_P sC_1R_1 I_2 + \alpha_P \beta_P sC_1R_1 I_3 + \alpha_P \beta_P \alpha'_N Yg_{m1}R_1 I_1}{s^2C_1C_2R_1R_2 + \alpha'_P \beta_P sC_1R_1 + \beta_N \alpha'_N Yg_{m1}R_2} \right] \tag{28}$$

$$V'_{out(TIM-Mode)} = R_3 \left[\frac{-\alpha_P [s^2C_1C_2R_1R_2 + \beta_P \alpha'_P sC_1R_1 + \beta_N \alpha'_N Yg_{m1}R_2] + \alpha_P \beta_P \alpha'_P sC_1R_1 I_2 + \alpha_P \beta_P sC_1R_1 I_3 + \alpha_P \beta_P \alpha'_N Yg_{m1}R_1 I_1}{s^2C_1C_2R_1R_2 + \alpha'_P \beta_P sC_1R_1 + \beta_N \alpha'_N Yg_{m1}R_2} \right] \tag{29}$$

$$f'_0 = \frac{1}{2\pi} \sqrt{\frac{\beta_N \alpha'_N Yg_{m1}}{C_1 C_2 R_1}} \tag{30}$$

$$Q' = \frac{R_2}{\alpha'_p \beta_p} \sqrt{\frac{\beta_N \alpha'_N Y g_{m1} C_2}{C_1 R_1}} \tag{31}$$

The sensitivities of ω'_0 and Q' with respect to the non-ideal gains and passive components are given below:

$$S_{g_{m1}}^{\omega'_0} = S_{\alpha'_N}^{\omega'_0} = S_{\beta_N}^{\omega'_0} = S_{\gamma}^{\omega'_0} = -S_{C_1}^{\omega'_0} = -S_{C_2}^{\omega'_0} = -S_{R_1}^{\omega'_0} = \frac{1}{2} \tag{32}$$

$$S_{g_{m1}}^{Q'} = S_{\alpha'_N}^{Q'} = S_{\beta_N}^{Q'} = S_{\gamma}^{Q'} = -S_{C_1}^{Q'} = S_{C_2}^{Q'} = -S_{R_1}^{Q'} = \frac{1}{2} \tag{33}$$

$$S_{R_2}^{Q'} = -S_{\alpha'_p}^{Q'} = -S_{\beta_p}^{Q'} = 1 \tag{34}$$

The sensitivities are low and have absolute values not higher than unity.

4.2. Non-Ideal Parasitic Analysis

The non-ideal model of the VD-EXCCII is presented in Figure 5. As can be deduced, the various parasitic resistance and capacitance appear in parallel with the input and output nodes of the device. The low impedance X_P and X_N nodes have a parasitic resistance and inductance in series with them. The associated parasitics at the X nodes can be quantified as $Z_{XP} = Z_{XN} = R_{X(N,P)} + sL_{X(N,P)}$. However, for the frequency of interest, the inductive effect can be ignored. The parasitic resistance and capacitance associated with the P, N, R_{ZP+} , R_{ZP-} , R_{ZN+} , R_{ZN-} , W, W_{C+} , W_{C-} and Z nodes are $R_N // C_N$, $R_P // C_P$, $R_{ZP+} // C_{ZP+}$, $R_{ZP-} // C_{ZP-}$, $R_{ZN+} // C_{ZN+}$, $R_{ZN-} // C_{ZN-}$, $R_{WC+} // C_{WC+}$, $R_{WC-} // C_{WC-}$ and $R_W // C_W$, their ideal values being equal to zero.

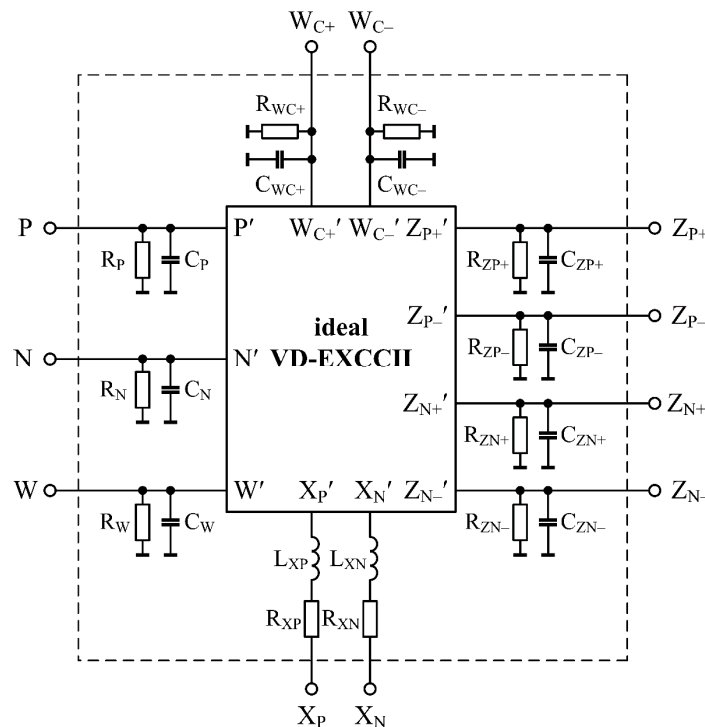


Figure 5. Non-ideal model of VD-EXCCII with parasitics.

Including the VD-EXCCII parasitics, the denominator of the filter transfer function will be modified as presented in Equation (35):

$$D(s) = s^2 + s \left[\frac{C'_1 R_{ZA} R'_2 + C'_1 R_{ZA} R'_W + C'_2 R'_W R'_2}{C'_1 C'_2 R'_W R_{ZA} R'_2} \right] + \frac{R'_1 R'_2 + R'_1 R'_W + g_{m1} R_{ZA} R'_2 R'_W}{C'_1 C'_2 R'_W R_{ZA} R'_2 R'_1} \tag{35}$$

where $C'_1 = (C_1 + C_{ZN-} + C_P)$, $C'_2 = (C_2 + C_{ZP-} + C_W)$, $R'_2 = (R_2 + R_{XP})$ and $R_{ZA} = R_{ZN-} // R_P$, $R'_W = R_{ZP-} // R_W$. The modified expressions of the frequency and quality factor including the various parasitic effects are presented in Equations (36) and (37):

$$f'_0 = \frac{1}{2\pi} \sqrt{\frac{R'_1 R'_2 + R'_1 R'_W + g_{m1} R_{ZA} R'_2 R'_W}{C'_1 C'_2 R'_W R_{ZA} R'_2 R'_1}} \tag{36}$$

$$Q' = \frac{1}{R'_2 C'_1 R_{ZA} + C'_1 R'_W R_{ZA} + C'_2 R'_W R'_2} \sqrt{\frac{C'_1 C'_2 R'_W R_{ZA} R'_2 (R'_1 R'_2 + R'_1 R'_W + g_{m1} R_{ZA} R'_2 R'_W)}{R'_1}} \tag{37}$$

To minimize the parasite effects the values of the passive components should be selected such that $C_1 \gg (C_{ZN-} \text{ and } C_P)$, $C_2 \gg (C_{ZP-} \text{ and } C_W)$. In addition, note that the resistors R_1 and R_2 are connected to the low impedance X terminals, so they will absorb the parasitic resistance present at XP and XN terminals since ($R_2 \gg R_{XP}$ and $R_1 \gg R_{XN}$).

5. Simulation and Validation

To validate the proposed mixed-mode filter, it was designed and simulated in Cadence Virtuoso design software. The VD-EXCCII was designed in 0.18 μm Silterra Malaysia technology at a supply voltage of ± 1.25 V. The width and length of the transistors used are given in Table 5. The layout of the VD-EXCCII as presented in Figure 6 was drawn using the nhp and php high-performance MOS transistors from the Silterra library, and the layout verification was done using the Calibre tool. The layout occupied a total area of $54.28 \times 22.80 \mu\text{m}^2$. The bias current of the OTA was fixed at 120 μA resulting in transconductance of 1.0321 mS. The important design parameters were extracted from post-layout simulations and are summarized in Table 6.

The proposed filter was tested by designing for a center frequency of 8.0844 MHz and quality factor of 1.015 by selecting the passive component as $R_1 = R_2 = R_3 = 1 \text{ k}\Omega$, $C_1 = C_2 = 20 \text{ pF}$ and $g_{m1} = 1.0321 \text{ mS}$. The power dissipation of the filter was found to be 5.76 mW. The five filter responses in VM, CM, TAM and TIM modes are presented in Figures 7–10.

Table 5. Width and length of the MOS transistors.

Transistors	Width (μm)	Length (μm)
M1–M2, M5–M6	1.8	0.36
M3–M4, M7–M9	5.8	0.36
M10–M14	1.8	0.72
M15–M18	3.06	0.36
M19–M22	4	0.36
M23, M25, M27, M33, M42, M44	2.16	0.36
M24, M26, M28, M32, M34, M30, M38, M36, M41, M43	0.72	0.72
M21, M31, M35, M37	1.08	0.72

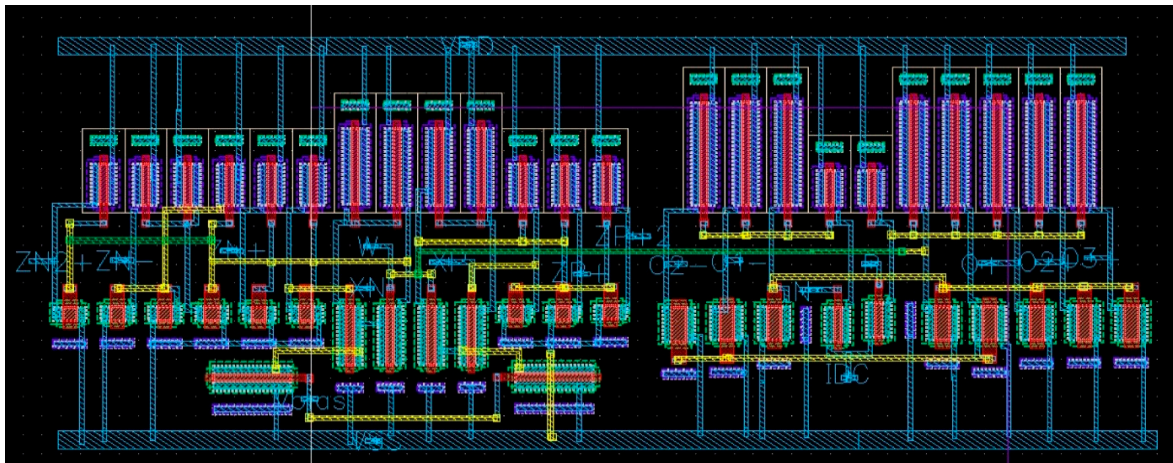


Figure 6. Layout of the VD-EXCCII.

Table 6. Performance metrics of VD-EXCCII.

Parameters	Silterra Technology ($V_{DD} = -V_{SS} = 1.25\text{ V}$)
Voltage gain (β_P, β_N)	0.96
Current gain (α_P, α_N)	0.9732
Current gain (α'_P, α'_N)	0.9687
Voltage transfer bandwidth ($V_{XP}/V_W, V_{XN}/V_W$)	2.28 GHz
Current transfer bandwidth ($I_{ZP+}/I_{XP}, I_{ZN+}/I_{XN}$)	1.344 GHz
Current transfer bandwidth ($I_{ZP-}/I_{XP}, I_{ZN-}/I_{XN}$)	1.29 GHz
DC voltage range (V_{XP}, V_{XN})	$\pm 720\text{ mV}$
DC current range (I_{ZP+}, I_{ZN+})	$\pm 240\ \mu\text{A}$
DC current range (I_{ZP-}, I_{ZN-})	$\pm 80\ \mu\text{A}$
X_P and X_N node resistance (R_{XP}, R_{XN})	$70\ \Omega$
Z_{P+} and Z_{N+} node resistance (R_{ZP+}, R_{ZN+})	$102.91\ \text{k}\Omega$
Z_{P-} and Z_{N-} node resistance (R_{ZP-}, R_{ZN-})	$102.71\ \text{k}\Omega$
W_{C+} and W_{C-} node resistance (R_{WC+}, R_{WC-})	$81.5\ \text{k}\Omega$
Static power dissipation	$3.18\ \text{mW}$ @ ($I_{Bias} = 50\ \mu\text{A}$)

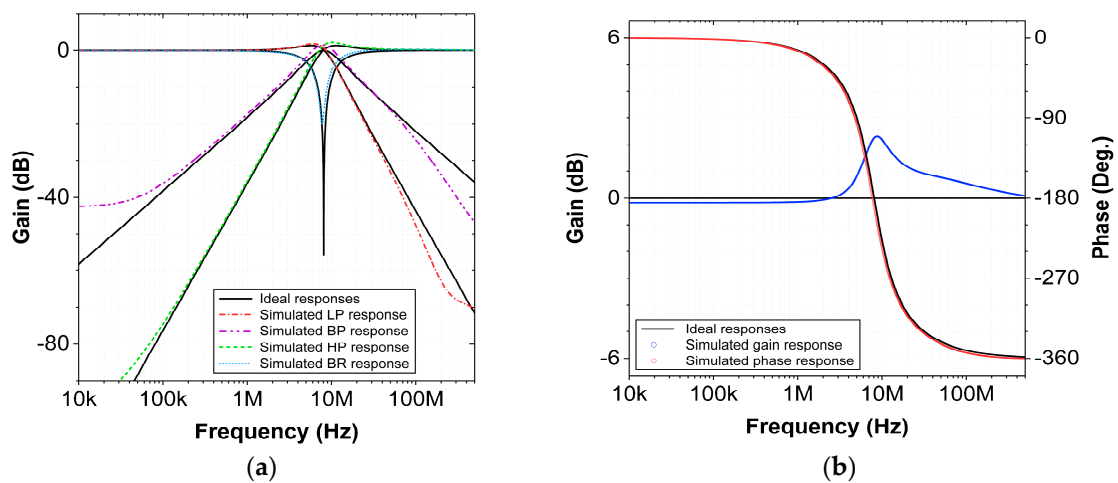


Figure 7. VM MISO configuration: (a) frequency responses of the LP, BP, HP and BR filter and (b) gain and phase responses of the AP filter.

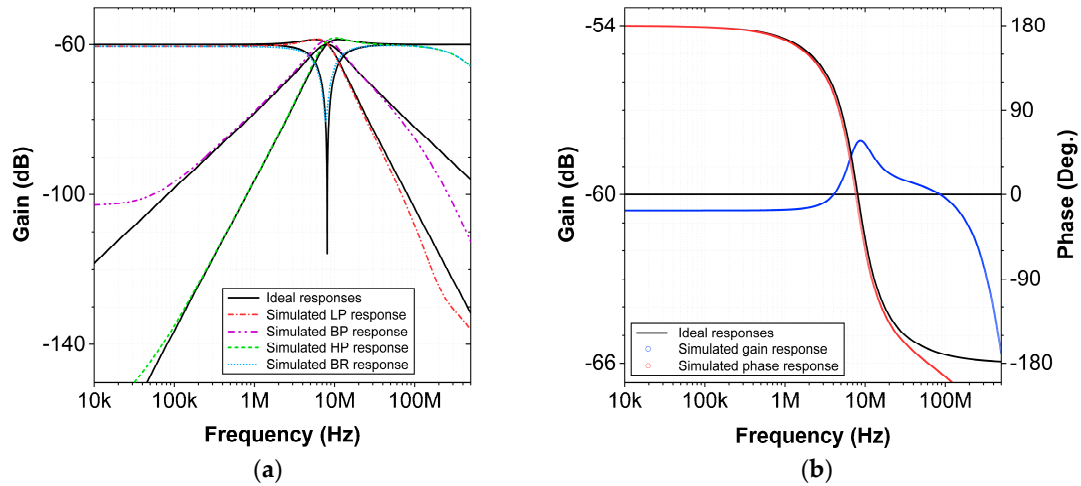


Figure 8. TAM MISO configuration: (a) frequency responses of the LP, BP, HP and BR filter and (b) gain and phase responses of the AP filter.

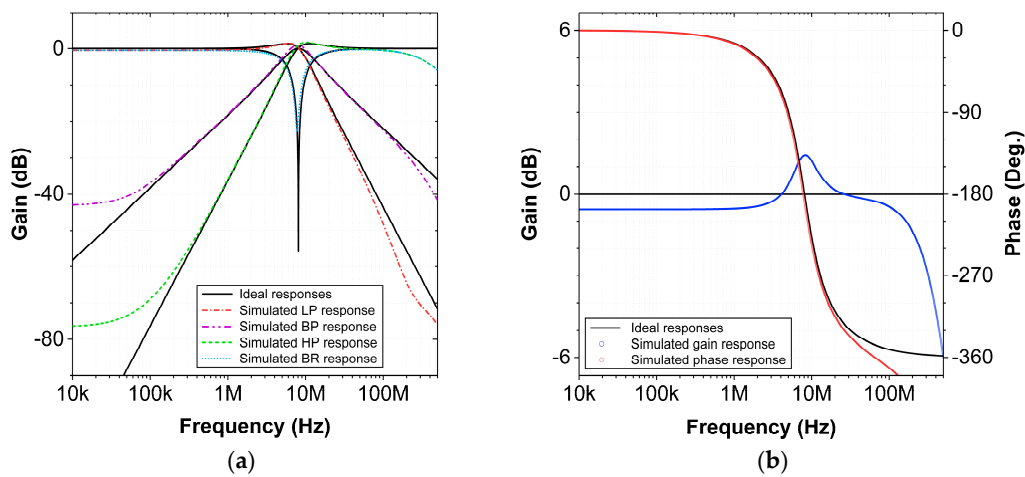


Figure 9. CM MISO configuration: (a) frequency responses of the LP, BP, HP, and BR filter and (b) gain and phase responses of the AP filter.

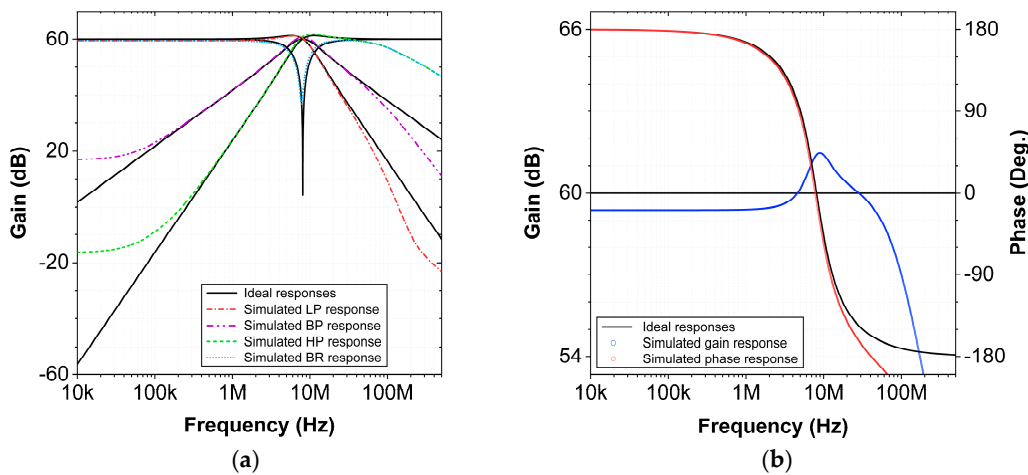


Figure 10. TIM MISO configuration: (a) frequency responses of the LP, BP, HP and BR filter and (b) gain and phase responses of the AP filter.

To examine the signal processing capability of the proposed universal filter, the transient analysis was carried out in VM mode for HP, LP and BP responses. A VM sinusoidal signal of 100 mV_{p-p} and a frequency of 8.0844 MHz was applied at the input, and the output was analyzed as presented in Figure 11. It can be inferred from the figure that the phase relation between the input and LP, BP and HP outputs of the filter are correct.

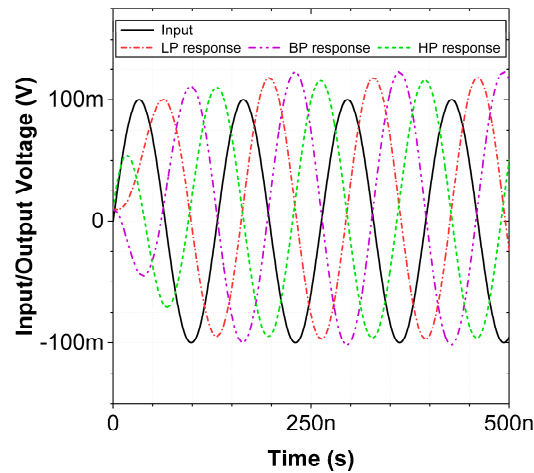


Figure 11. VM MISO configuration: transient analysis results for LP, BP and HP filter configurations.

In the presented filter, the quality factor can be set independent of the pole frequency of the filter, as is clear from Equations (17) and (18). The quality factor tunability was verified by analyzing the BP response in CM for different values of R_2 , as shown in Figure 12. It can be deduced from Figure 12b that the quality factor of the filter can be tuned linearly. The fitting equation using a linear regression with coefficient of determination $R^2 = 0.9832$, which indicates the fraction of the fitting values that are closest to the line of reference data, is given in Figure 12. The pole frequency of the proposed filter can be tuned by varying the bias current of the OTA, as can be inferred from Equation (17). The tuning property is validated by plotting the VM-AP response for the different values of the OTA bias current, as shown in Figure 13. The fitting equation using a power regression with $R^2 = 0.9962$ is given in Figure 13b.

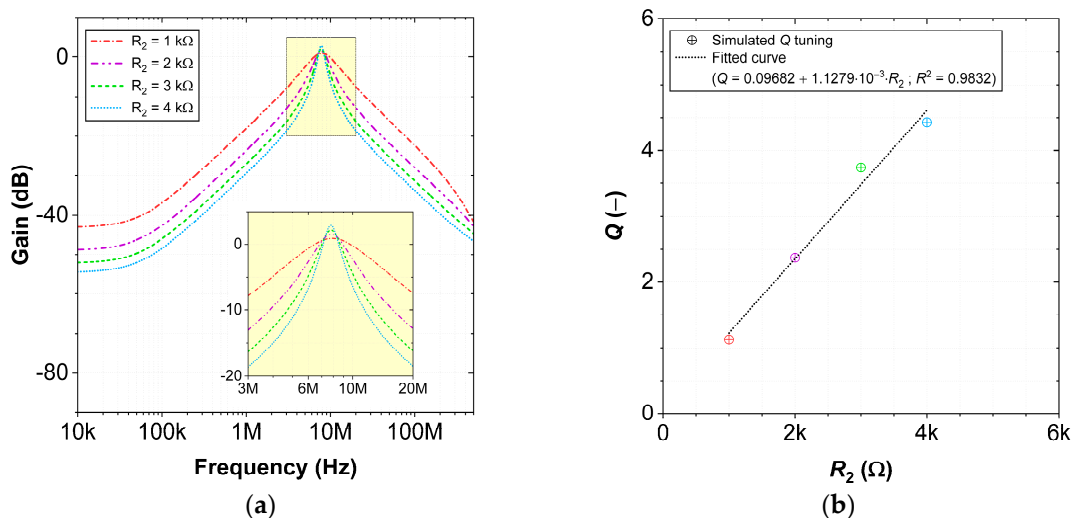


Figure 12. CM MISO configuration: (a) frequency responses and (b) quality factor tuning for different resistor values in BP filter.

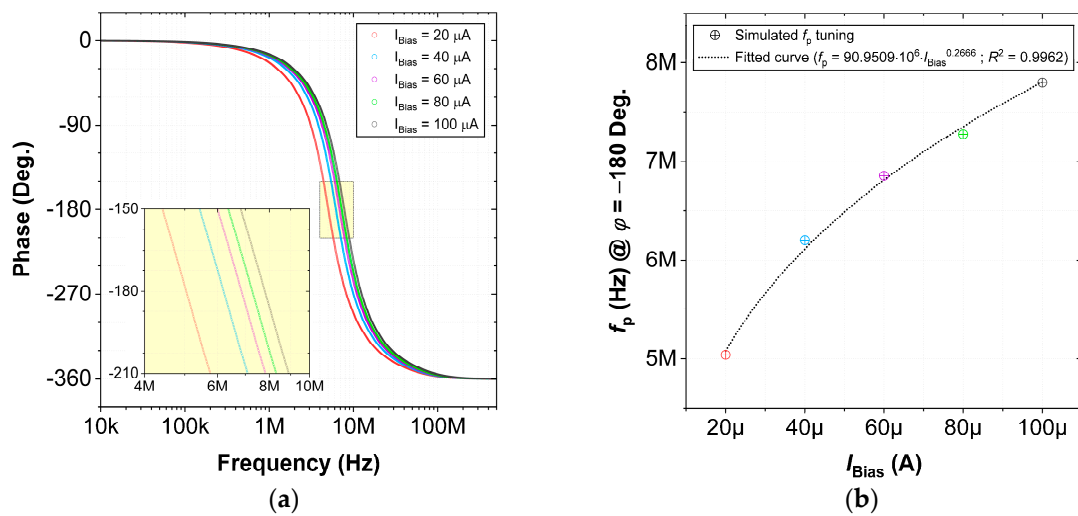


Figure 13. VM MISO configuration: (a) phase responses and (b) pole frequency tuning for different OTA bias current values for AP response.

To study the effect of process spread and the non-idealities of the capacitors employed on the performance of the designed filter, a Monte Carlo analysis is carried out for 200 runs. The Monte Carlo analysis results for the VM BP response are given in Figure 14. The results for CM AP configuration are given Figure 15. Corresponding histograms demonstrate the variations of the pole frequency at -180° . The results indicate that the frequency deviation of the filter is within acceptable limits. This further validates the robustness of the design.

The total harmonic distortion (THD) of the filter for LP and BP responses is plotted for different input signal amplitudes for VM as shown in Figure 16. The THD plot for CM-BP/LP is presented in Figure 17. The THD remains within acceptable limits ($\leq 7.5\%$) for appreciable input range.

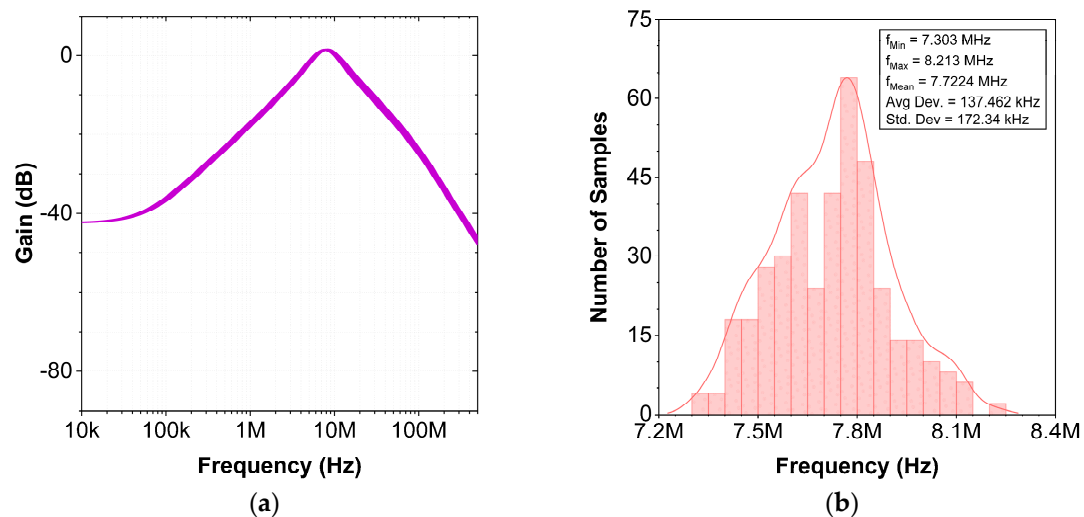


Figure 14. VM MISO configuration: (a) the Monte Carlo analysis results for BP response and (b) the corresponding histogram.

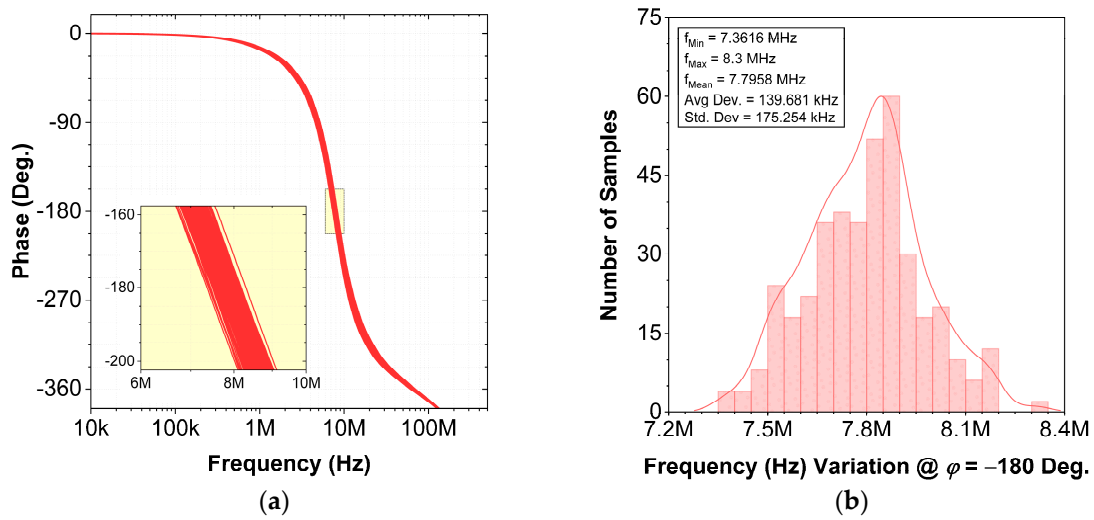


Figure 15. CM MISO configuration: (a) the Monte Carlo analysis results and (b) the corresponding histogram.

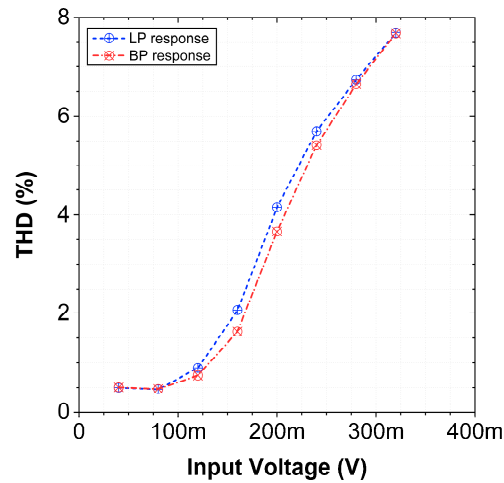


Figure 16. Total harmonic distortion of VM-BP and VM-LP.

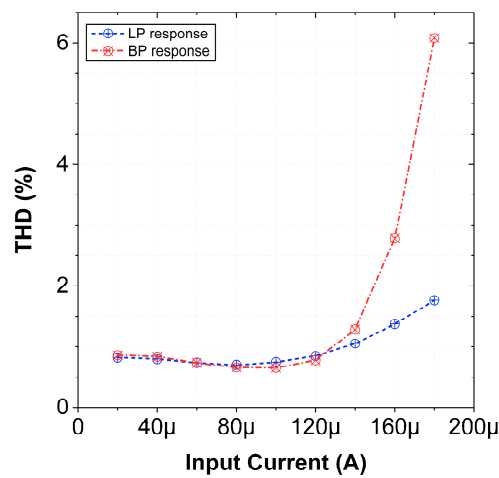


Figure 17. Total harmonic distortion of CM-BP.

The decrease in pole frequency of the filter due to rise in temperature can be attributed to the decrease in OTA transconductance. The main factors that influence the transconduct-

tance are the threshold voltage (V_t) and carrier mobility. V_t can be approximated as a linear function of temperature [45,46] given by Equation (38):

$$V_t(T) = V_t(T_0) + \alpha_{V_t}(T - T_0) \tag{38}$$

here, α_{V_t} denotes the threshold voltage temperature coefficient which, varies from $-1 \text{ mV}/^\circ\text{C}$ to $-4 \text{ mV}/^\circ\text{C}$ and T_0 is the reference temperature (300 K).

The dependence of carrier mobility on temperature is modelled by [46]:

$$\mu_N(T) = \mu_N(T_0) \left(\frac{T}{T_0} \right)^{\alpha_\mu} \tag{39}$$

where α_μ is the mobility temperature exponent considered as a constant approximately equal to 1.5. The Equations (38) and (39), show that the threshold voltage (V_t) and mobility (μ_N) exhibit a negative temperature dependence which explains the decrease in frequency with temperature, as shown in Figure 18 for CM AP response.

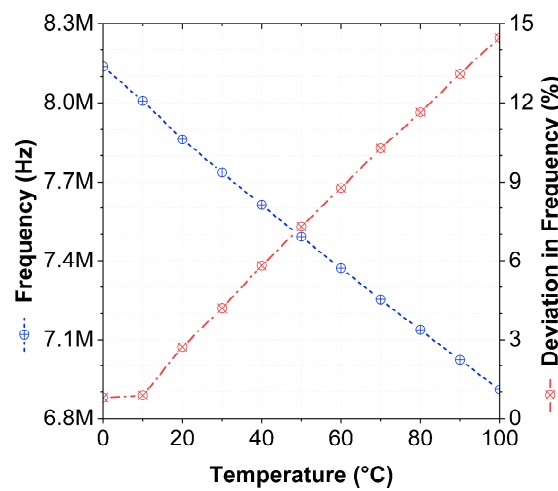


Figure 18. CM MISO configuration: variation of filter pole frequency with temperature and percentage of deviation from the designed frequency for AP response.

To validate the proposed CM-SIMO filter, it is designed for a center frequency of 6.4 MHz and quality factor of 1.015 by selecting passive component as $R_1 = R_2 = 2 \text{ k}\Omega$, $C_1 = C_2 = 20 \text{ pF}$ and $g_{m1} = 1.0321 \text{ mS}$. The five filter responses in CM mode are presented in Figure 19.

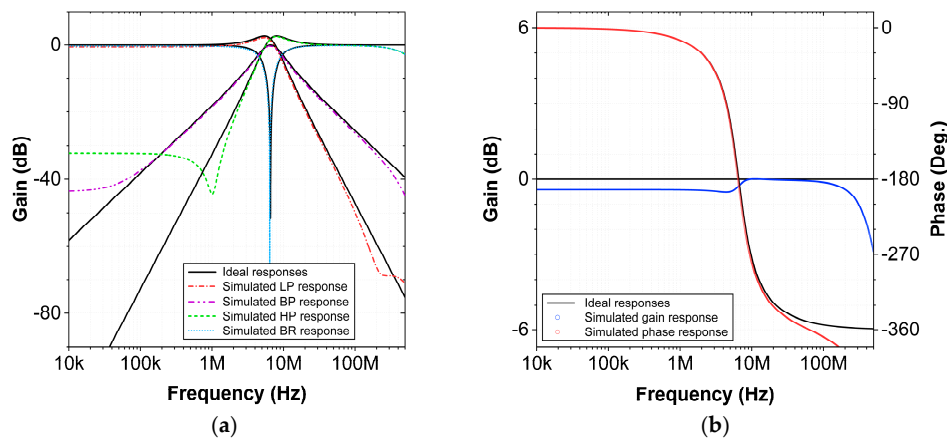


Figure 19. CM SIMO configuration: (a) frequency responses of the LP, BP, HP and BR filter and (b) gain and phase responses of the AP filter.

The time domain and Monte Carlo analysis results of the filter are presented in Figures 20 and 21, which verify the correct filter operation. The histogram depicted in Figure 21 demonstrates the variations of the pole frequency at -180° .

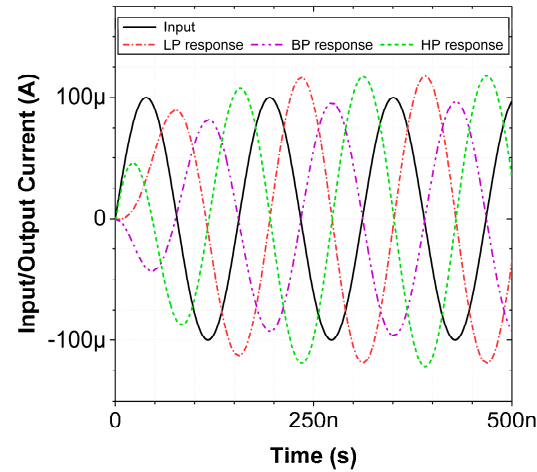


Figure 20. CM SIMO configuration: transient analysis results for LP, HP and BP filter configurations.

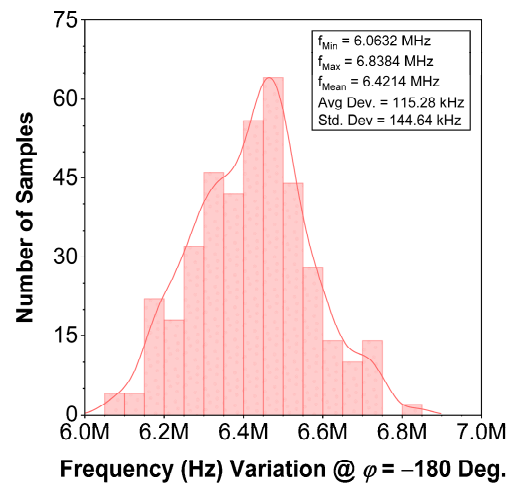


Figure 21. CM SIMO configuration: the Monte Carlo analysis results for AP configuration.

The Q factor tunability is tested for different values of resistor R_2 , as presented in Figure 22. The fitting equation using a linear regression with $R^2 = 0.9986$ is given in Figure 22b. Furthermore, the total harmonic distortion for different input current amplitudes is shown in Figure 23. It can be inferred that the THD remains approximately 2.5% for a considerable signal range.

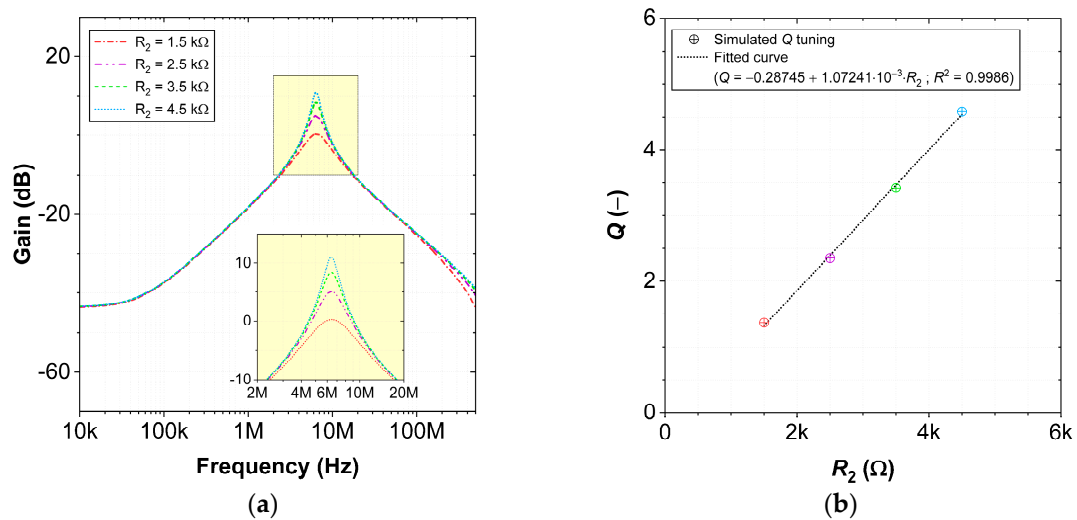


Figure 22. CM SIMO configuration: (a) frequency responses and (b) quality factor tuning for different resistor values in BP filter.

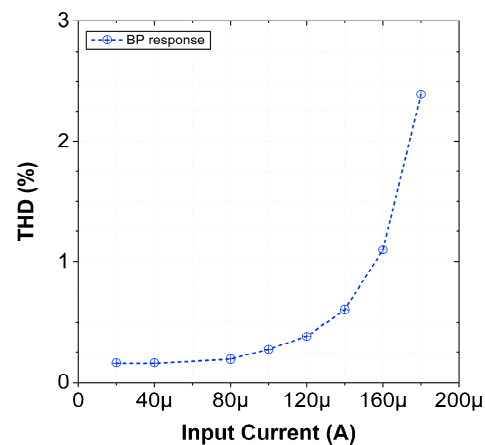


Figure 23. CM SIMO configuration: total harmonic distortion of CM-BP.

It can be concluded from the results that the characteristics of the AP filters have a slight imperfection, as all magnitude responses have a hump at the resonant frequency. This is caused by the frequency-dependent non-ideal current and voltage transfer gains and the parasitic resistances associated with the different nodes. All the mentioned non-idealities are discussed in detail in Section 4. It is also found that the linear range (dynamic range) of the circuit is mostly affected by small supply variations; however, the filter performance is not adversely affected.

To further bring out the merits of the proposed filter, a comparative analysis of the single ABBs-based mixed mode filters is carried out. It can be inferred from Table 7 that except [40], no other filter can provide all five filter responses in all four modes of operation. The latest presented filter in [47] is not a truly mixed mode and also suffers from use of negative and double input signals for filter response realization. The designs in [14,27,40,48] suffer from passive component matching requirements. The design in [48] requires a change in circuit configuration for realizing different responses, which is impractical. Although the proposed filter consumes more power compared with a few other designs, the power consumption of the filter can be reduced by redesigning the VD-EXCCII at low supply voltage and reduced bias currents.

Table 7. Comparative study of the mixed mode filters employing only a single ABB.

Reference	ABBs	Passive Components	Can Work in All Five Modes	Inbuilt Tunability	% THD in CM BP Configuration Till 50 μ A	Technology	Frequency of Operation	Power Consumption	Supply Voltage	Need of Negative and Double Input Signals	Independent Tunability of Q Without Affecting f_o	Passive Components Matching Condition
[14]	FDCCII	5	No	No	NA	0.25 μ m	3.316 MHz	NA	± 1.25 V	No	Yes	Yes
[25]	FDCCII	4	No	No	NA	0.18 μ m	10 MHz	NA	± 0.9 V	No	No	No
[27]	CFOA	5	No	No	NA	0.25 μ m	12.7 MHz	NA	± 1.25 V	Yes	Yes	Yes
[40]	MCCTA	2	Yes	Yes	less than 3	0.25 μ m	12.02 MHz	NA	± 1.25 V	No	Yes	Yes
[47]	EX-CCCII	3	No	Yes	less than 2.5	0.18 μ m	22.9 MHz	1.35 mW	± 0.5 V	Yes	Yes	No
[48]	CDBA	5	No	No	NA	AD844 model	3 MHz	NA	± 5 V	-	No	Yes
Proposed	VD-EXCCII	5	Yes	Yes	less than 1.5	0.18 μ m	8.084 MHz	5.76 mW	± 1.25 V	No	Yes	No

Note: 'NA' Not available; '-' Not applicable.

6. Filter Realization Using Macro Models of Commercially Available Integrated Circuits AD844 and LM13700

The proposed VD-EXCCII can be easily realized by commercially available ICs, the current feedback amplifier (AD844) and OTA (LM13700). The VD-EXCCII and the proposed filter circuit are realized using the PSpice macro model of the ICs to further test the feasibility of the proposed filter circuit. The setup for realizing the VD-EXCCII and the VM filter circuit depicted in Figure 3 is presented in Figure 24.

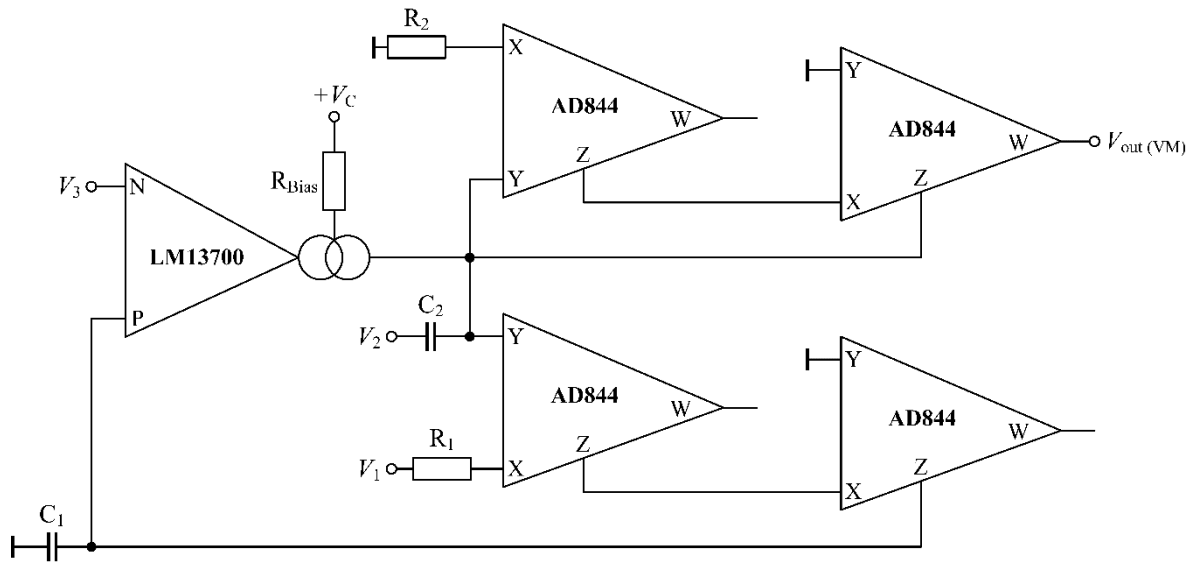


Figure 24. Scheme for the implementation of the VM filter depicted in Figure 3 using commercially available ICs.

The OTA transconductance is fixed at 2 mS by selecting $+V_C = 10\text{ V}$ and $R_{Bias} = 178.6\text{ k}\Omega$. The capacitors are selected equal to 1 nF and the resistors values are fixed as $R_1 = 1\text{ k}\Omega$ and $R_2 = 500\ \Omega$, resulting in $f_0 = 225\text{ kHz}$ and $Q = 0.707$. The AC analysis results of the filter are presented in Figure 25. The measured frequency is found to be 220.4 kHz, which translates into 2% error. A time domain analysis is also carried out for the VM-BP configuration. A sinusoidal signal of 40 mV_{p-p} at the 225 kHz frequency is applied at the input of the filter and the corresponding BP output is analyzed as shown in Figure 26, which establishes the correct functioning of the filter.

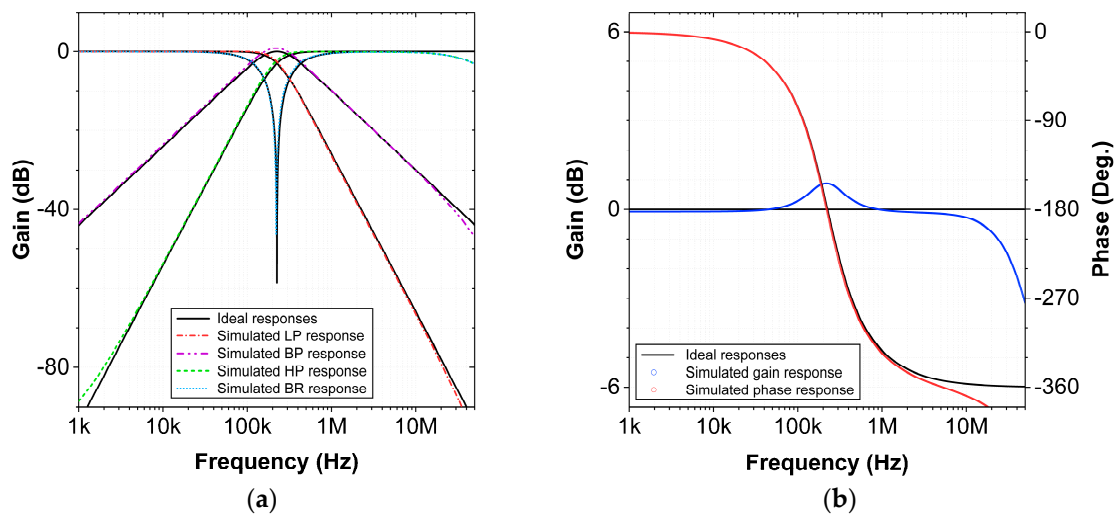


Figure 25. VM responses of the filter: (a) frequency responses of the LP, BP, HP and BR filter and (b) gain and phase responses of the AP filter.

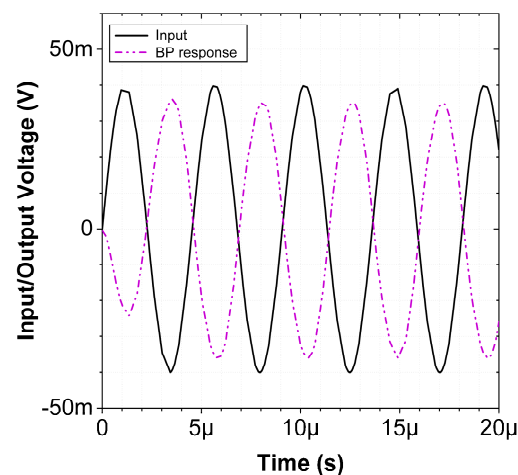


Figure 26. Time domain analysis result for the VM-BP response of the filter.

7. Conclusions

This paper presents a new single VD-EXCCII-based electronically tunable mixed-mode filter structure. The filter employs only one VD-EXCCII, three resistors and two capacitors. The mixed mode filter enjoys inbuilt tunability and can realize all five filter responses in all four modes of operation (VM, CM, TAM and TIM). A CM SIMO filter can also be derived from the presented minimum component mixed mode MISO filter topology. The detailed theoretical analysis, non-ideal gain analysis and parasitic study are given. The VD-EXCCII is designed in Cadence Virtuoso software and extensive post-layout simulations are carried out to examine and validate the proposed filter in all four modes of operation. The proposed filter has all the advantages mentioned in Section 3. The filter is designed for a frequency of 8.0844 MHz with a ± 1.25 V supply. The Monte Carlo analysis shows that the frequency deviation is within acceptable limits. Furthermore, the THD is within 5% for a considerable voltage/current input signal range. The power dissipation of the filter is found to be 5.76 mW. The VD-EXCCII and the mixed mode filter are also designed and tested using the models of commercially available ICs the AD844 and LM13700 in PSpice. The simulation results are found consistent with the theoretical predictions.

Author Contributions: Conceptualization, M.F., M.A.A. and J.S.; methodology, M.F., N.H., M.A.A. and J.S.; software, M.F.; validation, M.F. and M.A.A.; formal analysis, M.F., N.H. and J.S.; investigation, M.F., N.H. and J.S.; resources, M.A.A. and J.S.; data curation, M.F., N.H. and M.A.A.; writing—original draft preparation, M.F., N.H., M.A.A. and J.S.; writing—review and editing, M.F., N.H. and J.S.; visualization, N.H.; supervision, J.S.; project administration, M.F. and M.A.A.; funding acquisition, N.H., M.A.A. and J.S. All authors have read and agreed to the published version of the manuscript.

Funding: Part of this work was carried out at the Institute of Microengineering and Nanoelectronics (IMEN), University Kebangsaan Malaysia (UKM). This work is funded by the Ministry of Education Malaysia under grant (FRGS/1/2018/TK04/UKM/02/1) and AKU254:HICoE (Fasa II) ‘MEMS for Biomedical Devices (artificial kidney)’.

Acknowledgments: We would like to thank the anonymous reviewers for their insightful comments and suggestions.

Conflicts of Interest: The authors declare no conflict of interest. The funders had no role in the design of the study; in the collection, analyses or interpretation of data; in the writing of the manuscript, or in the decision to publish the results.

Abbreviations

The following abbreviations are used in this manuscript:

$\alpha_{P/N}, \alpha'_{P/N}$	Frequency dependent non-ideal current gains
α_{Vt}	Threshold voltage temperature coefficient
$\beta_{P/N}$	Frequency dependent non-ideal voltage gains
$\varepsilon_{gm}, \varepsilon'_{gm}$	Transconductance errors
$\varepsilon_{iP}, \varepsilon_{iN}$	Current tracking errors
$\varepsilon_{v(P,N)}$	Voltage tracking errors
γ, γ'	Frequency dependent non-ideal transconductance transfer gains
μ	Carrier mobility
ABB	Active building blocks
AP	All pass
BP	Band pass
BR	Band reject
C_{ox}	Gate oxide capacitance per unit area
CCII	Second-generation current conveyor
CFOA	Current feedback operational amplifier
CM	Current-mode
DDCC	Differential difference current conveyor
DPCCII	Digitally programmable second-generation current conveyor
DVCC	Differential voltage current conveyor
HP	High pass
ICCCII	Inverting second-generation current conveyor
L	Effective length of the channel
LP	Low pass
MISO	Multi input single output
MOCCCI	Multi output current controlled current conveyor
MOCCII	Multi output second-generation current conveyor
OTA	Operational transconductance amplifier
OTA	Operational transconductance amplifier
Q	Quality factor
SIMO	Single input multi output
TIM	Trans-impedance-mode
V_t	Threshold voltage
VDBA	Voltage differencing buffered amplifier
VDCC	Voltage differencing current conveyor
VD-EXCCII	Voltage Differencing Extra X Current Conveyor
VDTA	Voltage differencing transconductance amplifier
VDTA	Voltage differencing transconductance amplifier
VM	Voltage-mode
W	Effective channel width

References

- Mohan, P.A. *Current-Mode VLSI Analog Filters: Design and Applications*; Springer Science & Business Media: Berlin/Heidelberg, Germany, 2012.
- Ferri, G.; Guerrini, N.C. *Low-Voltage Low-Power CMOS Current Conveyors*; Springer Science & Business Media: Berlin/Heidelberg, Germany, 2003.
- Senani, R.; Bhaskar, D.; Singh, A. *Current Conveyors: Variants, Applications and Hardware Implementations*; Springer: Berlin/Heidelberg, Germany, 2014.
- Mohammad, F.; Sampe, J.; Shireen, S.; Ali, S.H.M. Minimum passive components based lossy and lossless inductor simulators employing a new active block. *AEU Int. J. Electron. Commun.* **2017**, *82*, 226–240. [[CrossRef](#)]
- Raut, R.; Swamy, M.N. *Modern Analog Filter Analysis and Design: A Practical Approach*; John Wiley & Sons: Hoboken, NJ, USA, 2010.
- Abuelma'Atti, M.T.; Bentrchia, A. A Novel mixed-mode CCII-based filter. *Act. Passiv. Electron. Compon.* **2004**, *27*, 197–205. [[CrossRef](#)]
- Abuelma'Atti, M.T.; Bentrchia, A.; Al-Shahrani, S.M. A novel mixed-mode current-conveyor-based filter. *Int. J. Electron.* **2004**, *91*, 191–197. [[CrossRef](#)]
- Abuelma'Atti, M.T. A Novel mixed-mode current-controlled current-conveyor-based filter. *Act. Passiv. Electron. Compon.* **2003**, *26*, 185–191. [[CrossRef](#)]
- Abuelma'Atti, M.T.; Bentrchia, A. A Novel mixed-mode OTA-C filter. *Frequenz* **2003**, *57*, 157–159. [[CrossRef](#)]
- Singh, V.K.; Singh, A.K.; Bhaskar, D.R.; Senani, R. Novel mixed-mode universal biquad configuration. *IEICE Electron. Express* **2005**, *2*, 548–553. [[CrossRef](#)]
- Shah, N.A.; Malik, M.A. Multifunction mixed-mode filter using FTFNs. *Analog. Integr. Circuits Signal Process.* **2006**, *47*, 339–343. [[CrossRef](#)]
- Pandey, N.; Paul, S.K.; Bhattacharyya, A.; Jain, S.B. A new mixed mode biquad using reduced number of active and passive elements. *IEICE Electron. Express* **2006**, *3*, 115–121. [[CrossRef](#)]

13. Ibrahim, M.A. Design and analysis of a mixed-mode universal filter using dual-output operational transconductance amplifiers (DO-OTAs). In Proceedings of the 2008 International Conference on Computer and Communication Engineering, Kuala Lumpur, Malaysia, 13–15 May 2008; pp. 915–918.
14. Lee, C.-N.; Chang, C.-M. Single FDCCII-based mixed-mode biquad filter with eight outputs. *AEU—Int. J. Electron. Commun.* **2009**, *63*, 736–742. [[CrossRef](#)]
15. Li, Z. Mixed-mode universal filter using MCCCII. *AEU—Int. J. Electron. Commun.* **2009**, *63*, 1072–1075. [[CrossRef](#)]
16. Minaei, S.; Ibrahim, M.A. A mixed-mode KHN-biquad using DVCC and grounded passive elements suitable for direct cascading. *Int. J. Circuit Theory Appl.* **2009**, *37*, 793–810. [[CrossRef](#)]
17. Chen, H.-P.; Liao, Y.-Z.; Lee, W.-T. Tunable mixed-mode OTA-C universal filter. *Analog. Integr. Circuits Signal Process.* **2008**, *58*, 135–141. [[CrossRef](#)]
18. Maheshwari, S.; Singh, S.; Chauhan, D. Electronically tunable low-voltage mixed-mode universal biquad filter. *IET Circuits Devices Syst.* **2011**, *5*, 149. [[CrossRef](#)]
19. Lee, C.-N.; Lee, C.-N. Multiple-mode OTA-C universal biquad filters. *Circuits Syst. Signal Process.* **2009**, *29*, 263–274. [[CrossRef](#)]
20. Pandey, N.; Paul, S.K.; Bhattacharyya, A.; Jain, S. Realization of generalized mixed mode universal filter using CCCII. *J. Act. Passive Electron. Devices* **2010**, *5*, 279–293.
21. Singh, S.; Maheshwari, S.; Chauhan, D. Electronically tunable current/voltage-mode universal biquad filter using CCCCTA. *Int. J. Recent Trends in Eng. Technol.* **2010**, *3*, 71–76.
22. Liao, W.-B.; Gu, J.-C. SIMO type universal mixed-mode biquadratic filter. *Indian J. Eng. Mater. Sci.* **2011**, *18*, 443–448.
23. Kumngern, M.; Junnapiya, S. Mixed-mode universal filter using OTAs. In Proceedings of the 2012 IEEE International Conference on Cyber Technology in Automation, Control, and Intelligent Systems (CYBER), Bangkok, Thailand, 27–31 May 2012; pp. 119–122.
24. Pandey, N.; Paul, S.K. Mixed mode universal filter. *J. Circuits Syst. Comput.* **2013**, *22*, 1250064. [[CrossRef](#)]
25. Kacar, F.; Kuntman, A.; Kuntman, H. Mixed-mode biquad filter employing single active element. In Proceedings of the 2013 IEEE 4th Latin American Symposium on Circuits and Systems (LASCAS), Cusco, Peru, 27 February–1 March 2013; pp. 1–4. [[CrossRef](#)]
26. Yeşil, A.; Kaçar, F. Electronically tunable resistorless mixed mode biquad filters. *Radioengineering* **2013**, *22*, 1016–1025.
27. Yuce, E. Fully integrable mixed-mode universal biquad with specific application of the CFOA. *AEU—Int. J. Electron. Commun.* **2010**, *64*, 304–309. [[CrossRef](#)]
28. Wang, L.; Wang, C.; Zhang, J.; Liang, X.; Jiang, S. A new mixed-mode filter based on MDDCCs. In Proceedings of the Seventh International Conference on Graphic and Image Processing (ICGIP 2015), Singapore, 23–25 October 2015; Volume 981717.
29. Lee, C.-N. Independently tunable mixed-mode universal biquad filter with versatile input/output functions. *AEU Int. J. Electron. Commun.* **2016**, *70*, 1006–1019. [[CrossRef](#)]
30. Lee, C.-N. Mixed-Mode Universal Biquadratic Filter with No Need of Matching Conditions. *J. Circuits Syst. Comput.* **2016**, *25*, 1650106. [[CrossRef](#)]
31. Chen, H.-P.; Yang, W.-S. Electronically Tunable Current Controlled Current Conveyor Transconductance Amplifier-Based Mixed-Mode Biquadratic Filter with Resistorless and Grounded Capacitors. *Appl. Sci.* **2017**, *7*, 244. [[CrossRef](#)]
32. Chamnanphai, V. Electronically Tunable SIMO Mixed-mode universal filter using VDTAs. *Przegląd Elektrotechniczny* **2017**, *1*, 209–213. [[CrossRef](#)]
33. Parvizi, M.; Taghizadeh, A.; Mahmoodian, H.; Kozehkanani, Z.D. A Low-Power Mixed-Mode SIMO Universal G_m-C Filter. *J. Circuits Syst. Comput.* **2017**, *26*, 1750164. [[CrossRef](#)]
34. Horng, J.-W.; Wu, C.-M.; Herencsar, N. Current-mode and transimpedance-mode universal biquadratic filter using two current conveyors. *Indian J. Eng. Mater. Sci.* **2017**, *24*, 461–468.
35. Cini, U.; Aktan, M. Dual-mode OTA based biquadratic filter suitable for current-mode applications. *AEU Int. J. Electron. Commun.* **2017**, *80*, 43–47. [[CrossRef](#)]
36. Chaturvedi, B.; Mohan, J.; Kumar, A. A New Versatile Universal Biquad Configuration for Emerging Signal Processing Applications. *J. Circuits Syst. Comput.* **2018**, *27*, 1850196. [[CrossRef](#)]
37. Tsukutani, T.; Yabuki, N. A DVCC-Based Mixed-Mode Biquadratic Circuit. *J. Electr. Eng.* **2018**, *6*, 52–56. [[CrossRef](#)]
38. Bhaskar, D.R.; Raj, A.; Kumar, P. Mixed-mode universal biquad filter using OTAs. *J. Circuits Syst. Comput.* **2019**, *29*, 2050162. [[CrossRef](#)]
39. Lee, C.-N.; Yang, W.-C. General Mixed-Mode Single-Output DDCC-based Universal Biquad Filter. *Int. J. Eng. Res.* **2020**, *9*, 744–749. [[CrossRef](#)]
40. Singh, S.V.; Tomar, R.S.; Chauhan, D.S. A new electronically tunable universal mixed-mode biquad filter. *J. Eng. Res.* **2016**, *4*, 1–21. [[CrossRef](#)]
41. Ettaghzouti, T.; Hassen, N.; Besbes, K. A Novel multi-input single-output mixed-mode universal filter employing second generation current conveyor circuit. In *Sensors, Circuits & Instrumentation Systems: Extended Papers 2017*; De Gruyter Oldenbourg: Berlin, Germany, 2018; Volume 6, pp. 53–64.
42. Maheshwari, S. Realization of Simple Electronic Functions Using EXCCII. *J. Circuits Syst. Comput.* **2017**, *26*, 1750171. [[CrossRef](#)]
43. Baker, R.J. *CMOS: Circuit Design, Layout, and Simulation*; John Wiley & Sons: Hoboken, NJ, USA, 2019.
44. Han, I.; Park, S. Voltage-controlled linear resistor by two MOS transistors and its application to active RC filter MOS integration. *Proc. IEEE* **1984**, *72*, 1655–1657. [[CrossRef](#)]
45. Tsividis, Y.; McAndrew, C. *Operation and Modeling of the MOS Transistor*; Oxford University Press: Oxford, UK, 2011.

46. Filanovsky, I.; Allam, A. Mutual compensation of mobility and threshold voltage temperature effects with applications in CMOS circuits. *IEEE Trans. Circuits Syst. I Fundam. Theory Appl.* **2001**, *48*, 876–884. [[CrossRef](#)]
47. Agrawal, D.; Maheshwari, S. High-Performance Electronically Tunable Analog Filter Using a Single EX-CCCII. *Circuits Syst. Signal. Process.* **2020**, 1–25. [[CrossRef](#)]
48. Koksal, M.; Oner, S.E.; Sagbas, M. A new second-order multi-mode multi-function filter using a single CDBA. In Proceedings of the 2009 European Conference on Circuit Theory and Design, Antalya, Turkey, 23–27 August 2009; pp. 699–702.